


AUTHOR QUERY FORM

	<p>Journal: Appl. Phys. Lett.</p> <p>Article Number: APL21-AR-05715</p>	<p>Please provide your responses and any corrections by annotating this PDF and uploading it to AIP's eProof website as detailed in the Welcome email.</p>
---	--	--

Dear Author,

Below are the queries associated with your article; please answer all of these queries before sending the proof back to AIP.

Article checklist: In order to ensure greater accuracy, please check the following and make all necessary corrections before returning your proof.

1. Is the title of your article accurate and spelled correctly?
2. Please check affiliations including spelling, completeness, and correct linking to authors.
3. Did you remember to include acknowledgment of funding, if required, and is it accurate?

Location in article	Query / Remark: click on the Q link to navigate to the appropriate spot in the proof. There, insert your comments as a PDF annotation.
<p style="color: blue;">AQ1</p> <p style="color: blue;">AQ2</p>	<p>Please check that the author names are in the proper order and spelled correctly. Also, please ensure that each author's given and surnames have been correctly identified (given names are highlighted in red and surnames appear in blue).</p> <p>Please define KI at first occurrence.</p> <p>Please confirm ORCID's are accurate. If you wish to add an ORCID for any author that does not have one, you may do so now. For more information on ORCID, see https://orcid.org/.</p> <p>S. E. Panasci-</p> <p>E. Schilirò - 0000-0001-8895-0825</p> <p>F. Migliore-</p> <p>M. Cannas - 0000-0001-8236-5043</p> <p>F. M. Gelardi-</p> <p>F. Roccaforte - 0000-0001-8632-0870</p> <p>F. Giannazzo - 0000-0002-0074-0469</p> <p>S. Agnello - 0000-0002-0346-8333</p> <hr/> <p>Please check and confirm the Funder(s) and Grant Reference Number(s) provided with your submission: Ministero dell'Istruzione, dell'Università e della Ricerca, Award/Contract Number FlagERA project ETMOS</p> <p>Please add any additional funding sources not stated above:</p>

Thank you for your assistance.

Substrate impact on the thickness dependence of vibrational and optical properties of large area MoS₂ produced by gold-assisted exfoliation

Cite as: Appl. Phys. Lett. **119**, 000000 (2021); doi: 10.1063/5.0062106

Submitted: 2 July 2021 · Accepted: 20 August 2021 ·

Published Online: 0 Month 0000



S. E. Panasci,^{1,2} E. Schilirò,¹ F. Migliore,³ M. Cannas,³ F. M. Gelardi,³ F. Roccaforte,¹ F. Giannazzo,^{1,a)} and S. Agnello^{1,3,4}

AFFILIATIONS

¹Institute for Microelectronic and Microsystems (CNR-IMM), Z.I. VIII Strada 5, 95121 Catania, Italy

²Department of Physics and Astronomy, University of Catania, Via Santa Sofia 64, 95123 Catania, Italy

³Department of Physics and Chemistry Emilio Segre', University of Palermo, Via Archirafi 36, 90123 Palermo, Italy

⁴ATeN Center, University of Palermo, Viale delle Scienze Ed. 18, 90128 Palermo, Italy

^{a)}Author to whom correspondence should be addressed: filippo.giannazzo@imm.cnr.it

ABSTRACT

The gold-assisted exfoliation is a very effective method to produce large-area (cm²-scale) membranes of molybdenum disulfide (MoS₂) for electronics. However, the strong MoS₂/Au interaction, beneficial for the exfoliation process, has a strong impact on the vibrational and light emission properties of MoS₂. Here, we report an atomic force microscopy, micro-Raman, and micro-photoluminescence (μ -PL) investigation of 2H-MoS₂ with variable thickness exfoliated on Au and subsequently transferred on an Al₂O₃/Si substrate. The E_{2g}-A_{1g} vibrational mode separation $\Delta\omega$ (typically used to estimate MoS₂ thickness) exhibits an anomalous large value ($\Delta\omega \approx 21.2$ cm⁻¹) for monolayer (1L) MoS₂ on Au as compared to the typical one ($\Delta\omega \approx 18.5$ cm⁻¹) measured on 1L MoS₂ on Al₂O₃. Such substrate-related differences, explained in terms of tensile strain and p-type doping arising from the MoS₂/Au interaction, were found to gradually decrease while increasing the number of MoS₂ layers. Furthermore, μ -PL spectra for 1L MoS₂ on Au exhibit a strong quenching and an overall redshift of the main emission peak at 1.79 eV, compared to the 1.84 eV peak for 1L MoS₂ on Al₂O₃. After PL spectra deconvolution, such redshift was explained in terms of higher trion/exciton intensity ratio, probably due to the higher polarizability of the metal substrate, as well as to the smaller equilibrium distance at the MoS₂/Au interface.

Published under an exclusive license by AIP Publishing. <https://doi.org/10.1063/5.0062106>

In the last few years, molybdenum disulfide (MoS₂) has been widely investigated, due to the broad range of potential applications in the fields of optoelectronics, nanoelectronics, sensing, and energy.¹⁻⁴ Several synthesis methods of MoS₂ films have been explored so far, including top-down and bottom-up methods.⁵ While the highest electronic quality MoS₂ is still produced by mechanical exfoliation, the micrometer size of the flakes obtained by this approach makes it unsuitable for practical applications. In this context, gold-assisted mechanical exfoliation has recently received increasing attention as an effective method to separate large area (cm²-scale) MoS₂ with excellent electronic quality from molybdenite crystals.⁶⁻⁹ Since the interaction between sulfur and Au atoms¹⁰ is stronger than the interlayer van der Waals (vdW) bonds in the layered crystal, ultrathin membranes [predominantly composed of monolayer (1L) MoS₂, but also containing bilayer (2L) and few-layer (FL) regions] are obtained simply pressing a

bulk MoS₂ stamp on a clean Au surface. These membranes can be subsequently transferred to insulating or semiconductor substrates to fabricate electronic/optoelectronic devices, showing performances comparable to those obtained with the best quality mechanically exfoliated MoS₂.⁷ Furthermore, as-exfoliated 1L MoS₂ on Au electrodes has been employed for memristor applications.¹¹ Finally, the Au-assisted exfoliation has been recently extended to a large number of layered crystals beyond MoS₂, including other transition metal dichalcogenides (MoSe₂, MoTe₂, 1T-MoTe₂, WS₂, WSe₂, WTe₂, TiS₂, TiSe₂, IrTe₂, SnS₂, SnSe₂, NbSe₂, NbTe₂, VSe₂, TaS₂, TaSe₂, PdSe₂), metal monochalcogenides (e.g., GaS), black-phosphorus, black-arsenic, metal trichlorides (RuCl₃), and magnetic compounds (Fe₃GeTe₂).¹² Hence, it represents a powerful method for the realization of artificial vdW heterostructures¹³⁻¹⁵ and hybrid 2D/bulk semiconductor devices.¹⁶⁻¹⁸

59 The strong MoS₂/Au interaction, which is beneficial for the
60 large-area exfoliation process, has a strong impact on the electronic,
61 vibrational, and light emission properties of MoS₂. Different studies
62 have been reported on the strain and doping of 1L MoS₂ induced by
63 the gold substrate.^{6,9} In this context, investigating the Au substrate
64 effects on MoS₂ vibrational and light emission properties as a function
65 of layers number deserves great interest. In particular, it is crucial to
66 evaluate the changes in these properties in the two main steps of Au-
67 assisted exfoliation, i.e., on as-exfoliated MoS₂ on Au and after transfer
68 to the final insulating substrate.

69 In this paper, the evolution of Raman and photoluminescence
70 (PL) spectra of large-area MoS₂ (first exfoliated on Au and subse-
71 quently transferred on an insulating Al₂O₃/Si substrate) was investi-
72 gated as a function of the number of layers, evaluated by atomic force
73 microscopy (AFM). We found that the separation $\Delta\omega$ between the in-
74 plane (E_{2g}) and out-of-plane (A_{1g}) vibrational modes, typically used
75 to estimate MoS₂ thickness, exhibits an anomalous large value
76 ($\Delta\omega \sim 21.2 \text{ cm}^{-1}$) for 1L MoS₂ on Au as compared to 1L MoS₂ trans-
77 ferred on Al₂O₃ ($\Delta\omega \sim 18.5 \text{ cm}^{-1}$). Such substrate-related difference
78 was found to gradually decrease while increasing the number of MoS₂
79 layers. Furthermore, PL spectra for 1L MoS₂ on Au exhibit a strong
80 quenching and an overall redshift of the main emission peak at
81 1.79 eV, compared to the 1.84 eV peak for 1L MoS₂ on Al₂O₃. Such
82 redshift was explained in terms of a higher trion/exciton intensity
83 ratio, probably due to the higher polarizability of the metal substrate,
84 as well as to the smaller equilibrium distance at the MoS₂/Au interface.

85 The Au samples employed for the exfoliation were prepared by
86 sequential deposition of the 10 nm Ni adhesion layer and the 15 nm
87 Au film on a SiO₂(900 nm)/Si substrate with DC magnetron sputtering
88 (Quorum Q300TDPLUS). A bulk MoS₂ stamp obtained by a freshly
89 cleaved 2H-MoS₂ crystal was pressed on the Au substrate immediately
90 after sputtering to prevent the adsorption of contaminants on the Au
91 surface that could reduce the exfoliation yield.⁶ The 2H-MoS₂ mem-
92 brane exfoliated on Au was finally transferred onto an insulating sub-
93 strate, consisting of 100 nm Al₂O₃ deposited on Si. The transfer
94 procedure consisted in the transfer of the Au/MoS₂ stack on the Al₂O₃
95 surface and the final etching of Au with a KI/I₂ solution.¹⁹

96 The thickness of MoS₂ was evaluated by tapping mode Atomic
97 Force Microscopy (AFM) using a DI3100 equipment by Bruker. The
98 morphology and phase images were acquired simultaneously using

sharp silicon tips with a curvature radius of 5 nm. Micro-Raman (μ -R) 99
and micro-Photoluminescence (μ -PL) spectra were obtained using a 100
Horiba Raman system with a confocal microscope (100 \times) and a laser 101
excitation wavelength of 532 nm. The laser power was filtered with a 102
neutral density (ND) filter at 1% for both spectroscopy methods. A 103
grating of 1800 lines/mm was used to acquire Raman spectra mean- 104
while a grating of 600 lines/mm to acquire PL spectra. All the spectra 105
were calibrated with respect to the Si peak at 520.7 cm^{-1} . 106

107 Figure 1(a) shows a photograph of the cm^2 -scale MoS₂ exfoliated 107
on the Au substrate, whereas two optical microscopy images at differ- 108
ent magnifications are reported in Figs. 1(b) and 1(c), respectively. 109
The variable optical contrast reveals that the MoS₂ membrane is pre- 110
dominantly composed of 1L areas, with the presence of FL regions 111
(violet color) and some Au uncovered areas. 112

113 After a preliminary identification of 1L and FL areas in the exfoli- 113
ated MoS₂ on Au by observation of the optical contrast, the number of 114
layers was precisely evaluated by tapping mode AFM. 115

116 Figure 2(a) shows an AFM image collected in a region compris- 116
ing both a bare Au area and MoS₂ covered regions with 1L, 2L, FL, 117
and multi-layer (bulk) thickness, indicated by different color dashed 118
lines. A phase map collected in the rectangular region indicated by the 119
white dashed line is also reported in Fig. 2(b). This image is comple- 120
mentary to the morphology, as it provides a clear identification of the 121
bare Au areas with respect to the MoS₂ covered ones, thanks to the 122
very different phase contrast. Figure 2(c) shows a representative height 123
line-scan across the region partially covered by 1L MoS₂, from which a 124
 $\sim 0.67 \text{ nm}$ step was evaluated, consistent with the nominal monolayer 125
thickness of 0.65 nm.¹ Furthermore, the 2L, FL, and bulk thicknesses 126
of the different areas in the morphological image are confirmed by the 127
line-scans reported in Figs. 2(d)–2(f), respectively. Preliminary optical 128
contrast inspection followed by AFM analyses was also employed to 129
identify regions with different thickness in the MoS₂ membrane trans- 130
ferred onto the Al₂O₃/Si substrate. 131

132 In the following, the impact of two different substrates (Au and 132
Al₂O₃) on the vibrational and optical emission properties of MoS₂ 133
areas with a different thickness has been investigated by μ -R and μ -PL 134
spectroscopy. Figures 3(a) and 3(b) report a comparison of typical 135
Raman spectra collected on 1L, 2L, FL, and bulk regions of the MoS₂ 136
membranes exfoliated on Au (a) and transferred onto Al₂O₃ (b). Here, 137
the FL region corresponds to four layers of MoS₂, while the bulk 138

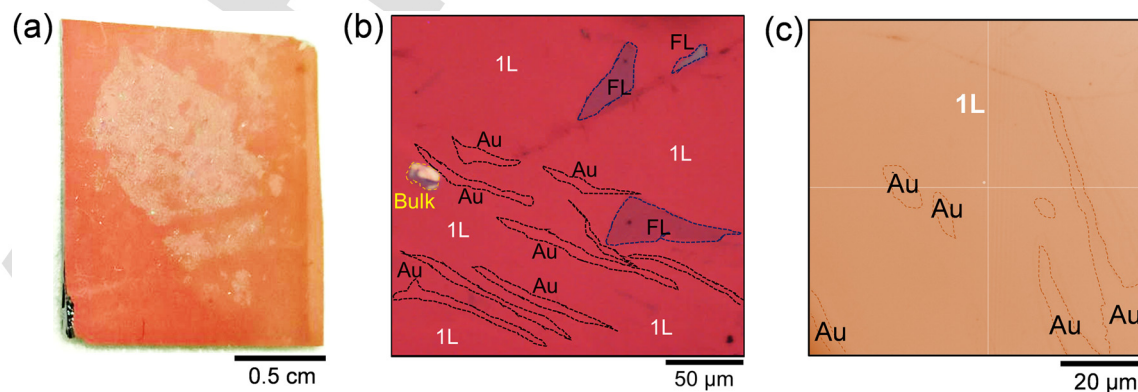


FIG. 1. (a) Photograph and (b) and (c) optical microscopy images at two different magnifications of the large area MoS₂ membrane on the Au substrate.

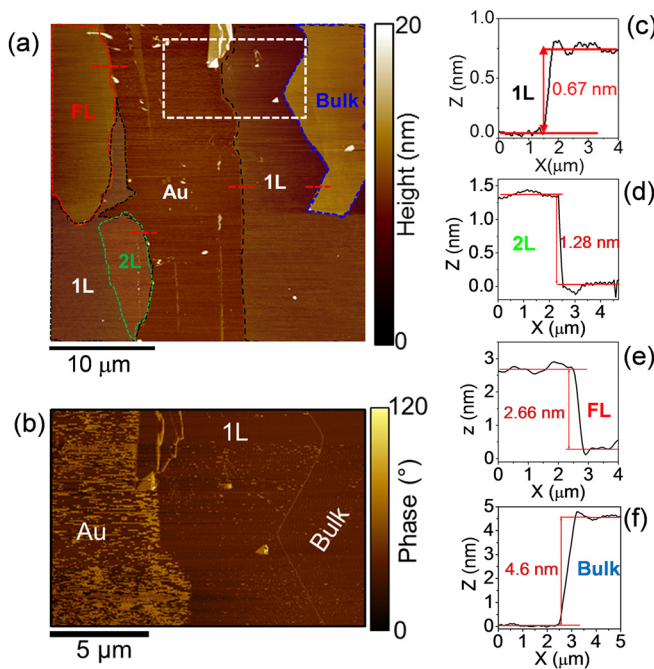


FIG. 2. (a) Morphological AFM image of a region of the exfoliated MoS₂ membrane on Au, containing areas with different MoS₂ thicknesses (1L, 2L, FL, and bulk) and bare Au areas. (b) Phase image corresponding to the white dashed rectangular region in (a), showing a different contrast between bare Au and MoS₂ covered regions. Height line scans from (c) 1L, (d) 2L, (e) FL, and (f) bulk MoS₂ areas in panel (a).

139 region was formed by ten layers of MoS₂. The characteristic in-plane
140 (E_{2g}) and of the out-of-plane (A_{1g}) vibrational modes are observed in
141 the spectral range from 370 to 420 cm^{-1} . All the spectra were normal-
142 ized with respect to the A_{1g} peak intensity. Furthermore, vertical
143 dashed lines, corresponding to the E_{2g} and A_{1g} peak positions for 1L
144 MoS₂ on Au and Al₂O₃, have been reported as a guide for the eye in
145 Figs. 3(a) and 3(b). It can be observed how both the individual
146 peak positions and their separation exhibit a very peculiar dependence
147 on the kind of substrate. While a value of $\Delta\omega \approx 18.5 \text{ cm}^{-1}$ is
148 measured for 1L MoS₂ transferred onto Al₂O₃, in the case of 1L MoS₂
149 exfoliated on Au, the E_{2g} and A_{1g} peaks exhibit a significant red- and
150 blueshift, respectively, resulting in a larger value of $\Delta\omega \approx 21.2 \text{ cm}^{-1}$.
151 Furthermore, a different behavior of the in-plane and out-of-plane
152 vibrational modes is observed on two different substrates with an
153 increase in the number of layers, as shown in Fig. 3(c).

154 For both substrates, the A_{1g} peak frequencies (filled and empty
155 triangles) exhibit a similar increasing trend with an increase in the
156 MoS₂ thickness. In particular, for thin MoS₂ membranes (1L–4L), the
157 A_{1g} peak on MoS₂/Au (filled triangles) is slightly blue-shifted with
158 respect to MoS₂/Al₂O₃ (empty triangles), whereas the two frequencies
159 converge to the same value for bulk samples. On the other hand, the
160 E_{2g} peak frequencies (filled and empty squares) show very different
161 trends on the two substrates. While the decreasing E_{2g} peak frequency
162 with an increase in the MoS₂ thickness on Al₂O₃ (empty squares) is
163 fully coherent with the reported literature results for MoS₂ on insulat-
164 ing substrates,²⁰ this peak exhibits an anomalous behavior in the Au

165 case (filled squares). In fact, for 1L MoS₂ on Au, E_{2g} is significantly red- 165
166 shifted (by $\sim 2 \text{ cm}^{-1}$) with respect to 1L MoS₂ on Al₂O₃. Its frequency 166
167 increases from 1L to 2L MoS₂ on Au and remains almost constant for 167
168 thicker membranes. It is noteworthy that, for bulk samples, the E_{2g} peak 168
169 frequencies exhibit the same values on the two substrates. Figure 3(d) 169
170 shows an increasing behavior of the peaks frequency difference $\Delta\omega$ as a 170
171 function of the number of MoS₂ layers for the two different substrates. 171
172 Furthermore, starting from a significantly larger value of $\Delta\omega \approx 21.2 \text{ cm}^{-1}$ 172
173 for 1L MoS₂ on Au as compared to $\Delta\omega \approx 18.5 \text{ cm}^{-1}$ for 1L MoS₂ on 173
174 Al₂O₃, the difference between the measured $\Delta\omega$ values is gradually 174
175 reduced with an increase in the number of layers, reaching approximately 175
176 the same value of $\sim 25 \text{ cm}^{-1}$ for bulk samples. 176

177 It is worth mentioning that the measured $\Delta\omega$ value in the Raman 177
178 spectra of MoS₂ is generally taken as a straightforward way to estimate 178
179 the number of layers. In particular, for 1L MoS₂ exfoliated/grown on 179
180 common insulating substrates (such as SiO₂), the reported values of 180
181 the separation $\Delta\omega$ between E_{2g} and A_{1g} vibrational peaks can range 181
182 from ~ 18 to $\sim 20 \text{ cm}^{-1}$.²⁰ Hence, the value of 18.5 cm^{-1} for our 1L 182
183 MoS₂ exfoliated on Au and transferred to the Al₂O₃/Si substrate is in 183
184 the range of the commonly reported literature values. In particular, it 184
185 is very close to the value measured on 1L MoS₂ flakes directly exfoliat- 185
186 ed on Al₂O₃.²¹ On the other hand, for as-exfoliated 1L MoS₂ on Au, 186
187 an anomalously large value of $\Delta\omega = 21.2 \text{ cm}^{-1}$ is measured. Since the 187
188 Au-assisted exfoliation is a very clean process (simply achieved by 188
189 pressing the fresh surface of the bulk MoS₂ stamp onto the as- 189
190 deposited Au film), the large $\Delta\omega$ value cannot be explained by the 190
191 presence of impurities at the MoS₂/Au interface or on the MoS₂ sur- 191
192 face. On the other hand, its origin is the strong interaction between 192
193 MoS₂ and the Au substrate.¹⁹ 193

194 The interaction with the substrate, particularly relevant in the 194
195 case of ultrathin MoS₂ membranes, can result in both the doping 195
196 effects, associated with charge transfer phenomena, and in tensile or 196
197 compressive strain effects. The E_{2g} and A_{1g} Raman modes are known 197
198 to be related to the strain (ϵ) and doping (n) of MoS₂ membranes. In 198
199 particular, a quantification of the strain type (tensile/compressive) and 199
200 percentage and of the doping type and carrier density induced on 1L 200
201 MoS₂ by the gold and Al₂O₃ substrates has been carried out using the 201
202 following equations: 202

$$\omega_{E_{2g}} = \omega_{E_{2g}}^0 - 2\gamma_{E_{2g}} \omega_{E_{2g}}^0 \epsilon + k_{E_{2g}} n, \quad (1)$$

$$\omega_{A_{1g}} = \omega_{A_{1g}}^0 - 2\gamma_{A_{1g}} \omega_{A_{1g}}^0 \epsilon + k_{A_{1g}} n. \quad (2)$$

203 Here, $\gamma_{E_{2g}} = 0.68$ and $\gamma_{A_{1g}} = 0.21$ are the two Grüneisen parameters, 203
204 correlating the strain ϵ and the E_{2g} and A_{1g} peaks positions for 1L 204
205 MoS₂,²³ while $k_{E_{2g}} = -0.33 \times 10^{-13} \text{ cm}$ and $k_{A_{1g}} = -2.2 \times 10^{-13} \text{ cm}$ 205
206 are the shift rates of the Raman peaks as a function of the electron den- 206
207 sity n (in cm^{-2}).²² Furthermore, $\omega_{E_{2g}}^0 = 385 \text{ cm}^{-1}$ and $\omega_{A_{1g}}^0 = 405 \text{ cm}^{-1}$ 207
208 are the literature values of the E_{2g} and A_{1g} peaks frequen- 208
209 cies for a suspended 1L MoS₂ membrane under 532 nm excitation,²³ 209
210 which represents the best approximation of an ideally unstrained 210
211 and undoped 1L MoS₂. According to Eqs. (1) and (2), a biaxial 211
212 tensile strain $\epsilon \approx 0.21\%$ and a p-type doping $n \approx -0.25 \times 10^{13} \text{ cm}^{-2}$ 212
213 were estimated for 1L MoS₂ exfoliated on Au, which was converted 213
214 into a biaxial compressive strain $\epsilon \approx -0.25\%$ and n-type doping n 214
215 $\approx 0.5 \times 10^{13} \text{ cm}^{-2}$ after transfer to the Al₂O₃ substrate. Such n-type 215
216 behavior is consistent with the unintentional doping type commonly 216
217 reported for exfoliated or CVD-grown MoS₂, which has been 217

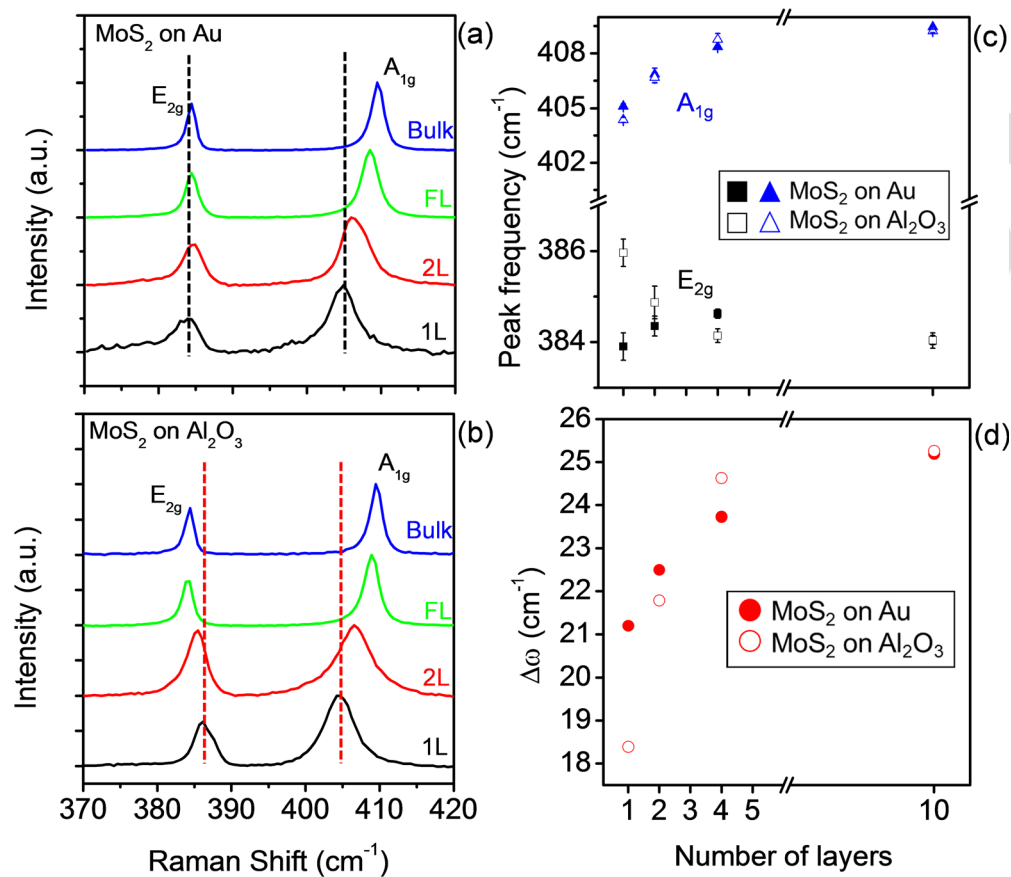


FIG. 3. Typical Raman spectra of exfoliated MoS₂ on the Au substrate (a) and transferred onto Al₂O₃/Si (b) measured on 1L, 2L, FL, and bulk MoS₂ regions. The black (red) dashed lines indicate the E_{2g} and A_{1g} peaks frequencies for 1L MoS₂ on Au (Al₂O₃). (c) Behavior of the E_{2g} and A_{1g} peak frequencies as a function of the number of layers for MoS₂ on Au (filled squares and triangles) and for MoS₂ on Al₂O₃ (open squares and triangles). (d) Plot of the peaks frequency difference $\Delta\omega$ as a function of the number of layers for MoS₂ on Au (filled red circles) and MoS₂ on Al₂O₃ (empty red circles).

218 associated with the presence of defects (e.g., sulfur vacancies) or other
 219 impurities in the MoS₂ lattice.²⁴ In the case of 1L MoS₂ on Au, a strong
 220 electron transfer to the substrate is guessed, which overcompensates
 221 the native n-type doping, resulting in a net p-type behavior.
 222 Furthermore, the tensile strain for 1L MoS₂ on Au can be ascribed to
 223 the lattice mismatch between MoS₂ and the Au surface, mostly exposing
 224 the lattice (111) orientation.^{25,26}

225 Besides influencing the vibrational properties, the interaction
 226 with the substrate is expected to have an impact also on the optical
 227 emission behavior of MoS₂. Figures 4(a) and 4(b) illustrate the results
 228 of μ -PL analyses performed at room temperature under 532 nm excitation
 229 on MoS₂ areas with different thickness on the Au and Al₂O₃
 230 substrates. In particular, the black, red, and green lines represent the
 231 PL spectra for 1L, FL, and bulk MoS₂. In order to perform a reliable
 232 comparison of the PL signal on the two different substrates, for each
 233 spectrum the intensities were normalized to the intensity of the MoS₂
 234 Raman peaks. In this way, the comparison of the PL intensities
 235 between Figs. 4(a) and 4(b) demonstrates a quenching (~ 4 times)
 236 of the emission yield for 1L MoS₂ exfoliated on Au as compared to 1L
 237 MoS₂ transferred onto Al₂O₃. A reduction in the relative PL intensities

238 when increasing the MoS₂ thickness from 1L to FL was consistently
 239 observed on both kinds of substrates, with the intensity approaching
 240 to zero in bulk samples according to the indirect bandgap. Looking
 241 more in detail at PL emission for 1L MoS₂, for both substrates, the PL
 242 spectra exhibit a main intense peak at lower energy and another
 243 weaker peak at higher energy, associated with the MoS₂ band splitting
 244 due to spin-orbit coupling.^{27,28} While the main peak for 1L MoS₂ on
 245 Al₂O₃ is located at 1.84 eV, similarly to what typically reported on
 246 other insulating substrates,²⁹ a significant redshift to 1.79 eV is
 247 observed for 1L MoS₂ on the Au substrate. To get a deeper insight
 248 in the PL emission mechanisms of 1L MoS₂ on the two different
 249 substrates, a deconvolution of two representative spectra has been carried
 250 out, as reported in Figs. 4(c) and 4(d). In both cases, the best fit was
 251 obtained considering three Gaussian peaks, which were associated
 252 with a trionic contribution T (green dashed line), and two excitonic
 253 contributions, i.e., the exciton A⁰ (blue) and the exciton B (gray).^{30–32}
 254 Differently from neutral excitons, consisting of a bound electron/hole
 255 pair, trions are charged quasiparticles formed by two electrons and a
 256 hole.³⁰ It is noteworthy that, while the exciton peak A⁰ at 1.84 eV rep-
 257 represents the main PL contribution for 1L MoS₂ on Al₂O₃, the trion

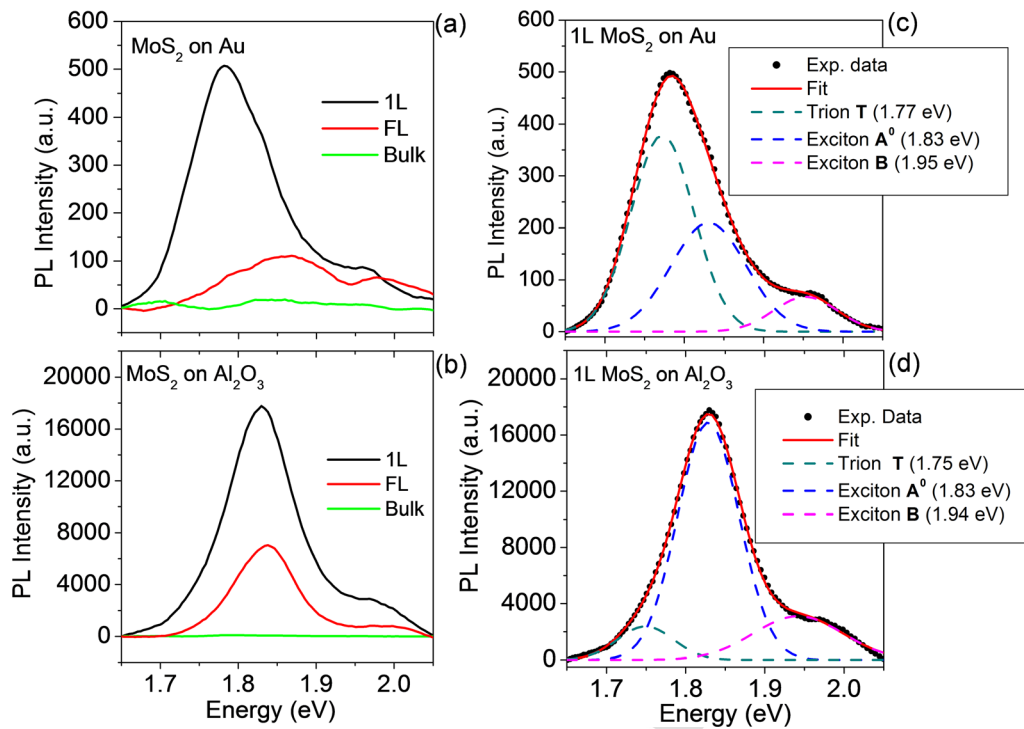


FIG. 4. Photoluminescence spectra under 532 nm excitation for 1L, FL, and bulk MoS₂ on Au (a) and Al₂O₃ substrates (b). Deconvolution of PL spectra for (c) 1L MoS₂ on Au and (d) 1L MoS₂ on Al₂O₃. Three different components were identified: the trion peak T, the exciton peak A⁰, and the exciton peak B.

258 peak T at 1.78 eV appears to be the dominant one in the case of 1L
 259 MoS₂ on Au. Finally, the B exciton peak at 1.94 eV for 1L MoS₂ on
 260 Al₂O₃ exhibits a significantly higher full width at half maximum
 261 (FWHM) with respect to the corresponding peak (at 1.96 eV) for 1L
 262 MoS₂ on Au. As indicated in the labels of Figs. 4(c) and 4(d), the T, A⁰
 263 and B peaks obtained by the deconvolution are slightly blue-shifted in
 264 the case of 1L MoS₂ on Au with respect to 1L MoS₂ on Al₂O₃. However,
 265 the overall redshift of the PL spectra for 1L MoS₂ on Au is due to the
 266 higher intensity of the trion contribution. As reported in recent theoretical
 267 studies,^{33,34} this effect can be ascribed to the high polarizability of the
 268 metal substrate and to the low MoS₂/Au equilibrium distance enhancing
 269 the trion population and at the same time quenching the overall emis-
 270 sion amplitude.⁶ It is noteworthy that, in the case of FL MoS₂ on Au
 271 [Fig. 4(a)], the main PL peak appears to be broader and blue-shifted
 272 with respect to the monolayer one, and its energy is closer to that of FL
 273 MoS₂ on Al₂O₃. This observation suggests that the increase in the MoS₂
 274 thickness results in a reduced effect of the substrate not only on vibra-
 275 tional properties but also on PL emission.

276 In conclusion, we have deeply investigated the substrate effects
 277 on the Raman and PL emission properties of cm²-wide MoS₂ mem-
 278 branes exfoliated on Au and subsequently transferred on an insulating
 279 Al₂O₃/Si substrate. For as-exfoliated 1L MoS₂ on Au, Raman spectra
 280 showed an anomalous large value of $\Delta\omega \approx 21.2 \text{ cm}^{-1}$ (due to the ten-
 281 sile strain and p-type doping induced by the substrate) as compared to
 282 the typical one ($\sim 18.5 \text{ cm}^{-1}$) measured after the transfer of 1L MoS₂
 283 on Al₂O₃ and complete removal of Au. Such substrate-related differ-
 284 ences were found to gradually decrease while increasing the number of
 285 MoS₂ layers. These results also have practical implications, indicating

that Raman spectroscopy should be used in combination with other
 physical characterizations (e.g., AFM or transmission electron micro-
 copy) to unambiguously evaluate the number of MoS₂ layers.
 Furthermore, PL spectra for 1L MoS₂ on Au exhibit a strong quench-
 ing and an overall redshift of the main emission peak at 1.79 eV, com-
 pared to the 1.84 eV peak position for 1L MoS₂ on Al₂O₃. Such
 redshift was explained in terms of a higher trion/exciton intensity
 ratio, indicating how the relative population of quasiparticles gener-
 ated under light excitation is significantly affected by the 1L MoS₂/Au
 interaction.

These results will be relevant in view of the widespread applica-
 tions of large-area MoS₂ membranes produced by the gold-assisted
 exfoliation in electronics and optoelectronics.

S. Di Franco (CNR-IMM) is acknowledged for the expert
 technical assistance in sample preparation. This work has been
 supported, in part, by MUR in the framework of the FlagERA-
 JTC2019 project ETMOS. Part of this work has been carried out in
 the Italian Infrastructure Beyond-Nano Upgrade.

DATA AVAILABILITY

The data that support the findings of this study are available
 from the corresponding author upon reasonable request.

REFERENCES

- ¹B. Radisavljevic, A. Radenovic, J. Brivio, V. Giacometti, and A. Kis, *Nat. Nanotechnol.* **6**, 147–150 (2011).
- ²O. Lopez-Sanchez, D. Lembke, M. Kayci, A. Radenovic, and A. Kis, *Nat. Nanotechnol.* **8**, 497–501 (2013).

- 313 ³Z. Yin, H. Li, H. Li, L. Jiang, Y. Shi, Y. Sun, G. Lu, Q. Zhang, X. Chen, and H. Zhang, *ACS Nano* **6**, 74–80 (2012). 349
- 314 ⁴F. Giannazzo, *Nat. Electron.* **2**, 54–55 (2019). 350
- 315 ⁵J. Sun, X. Li, W. Guo, M. Zhao, X. Fan, Y. Dong, C. Xu, J. Deng, and Y. Fu, *Crystals* **7**, 198 (2017). 351
- 316 ⁶M. Velický, G. E. Donnelly, W. R. Hendren, S. McFarland, D. Scullion, W. J. I. DeBenedetti, G. C. Correa, Y. Han, A. J. Wain, M. A. Hines, D. A. Muller, K. S. Novoselov, H. D. Abruña, R. M. Bowman, E. J. G. Santos, and F. Huang, *ACS Nano* **12**, 10463–10472 (2018). 352
- 317 ⁷S. B. Desai, S. R. Madhvapathy, M. Amani, D. Kiriya, M. Hettick, M. Tosun, Y. Zhou, M. Dubey, J. W. Ager III, D. Chrzan, and A. Javey, *Adv. Mater.* **28**, 4053–4058 (2016). 353
- 318 ⁸G. Z. Magda, J. Petó, G. Dobrik, C. Hwang, L. P. Biró, and L. Tapasztó, *Sci. Rep.* **5**, 14714 (2015). 354
- 319 ⁹M. Velický, A. Rodriguez, M. Bouša, A. V. Krayev, M. Vondráček, J. Honolka, M. Ahmadi, G. E. Donnelly, F. Huang, H. D. Abruña, K. S. Novoselov, and O. Frank, *J. Phys. Chem. Lett.* **11**, 6112–6118 (2020). 355
- 320 ¹⁰H. Häkkinen, *Nat. Chem.* **4**, 443 (2012). 356
- 321 ¹¹S. M. Hus, R. Ge, P.-A. Chen, L. Liang, G. E. Donnelly, W. Ko, F. Huang, M.-H. Chiang, A.-P. Li, and D. Akinwande, *Nat. Nanotechnol.* **16**, 58–62 (2021). 357
- 322 ¹²Y. Huang, Y.-H. Pan, R. Yang, L.-H. Bao, L. Meng, H.-L. Luo, Y.-Q. Cai, G.-D. Liu, W.-J. Zhao, Z. Zhang, L.-M. Wu, Z.-L. Zhu, M. Huang, L.-W. Liu, L. Liu, P. Cheng, K.-H. Wu, S.-B. Tian, C.-Z. Gu, Y.-G. Shi, Y.-F. Guo, Z. G. Gang, J.-P. Hu, L. Zhao, G.-H. Yang, E. Sutter, P. Sutter, Y.-L. Wang, W. Ji, X.-J. Zhou, and H.-J. Gao, *Nat. Commun.* **11**, 2453 (2020). 358
- 323 ¹³F. Liu, W. Wu, Y. Bai, S. H. Chae, Q. Li, J. Wang, J. Hone, and X.-Y. Zhu, *Science* **367**, 903–906 (2020). 359
- 324 ¹⁴Y. Chen and M. Sun, *Nanoscale* **13**, 5594 (2021). 360
- 325 ¹⁵J. Fan, J. Song, Y. Cheng, and M. Sun, *Results Phys.* **24**, 104110 (2021). 361
- 326 ¹⁶F. Giannazzo, G. Greco, F. Roccaforte, and S. S. Sonde, *Crystals* **8**, 70 (2018). 362
- 327 ¹⁷A. Gnisci, G. Faggio, L. Lancellotti, G. Messina, R. Carotenuto, E. Bobeico, P. Delli Veneri, A. Capasso, T. Dikonimos, and N. Lisi, *Phys. Status Solidi A* **216**, 1800555–1800559 (2019). 363
- 328 ¹⁸F. Giannazzo, G. Greco, E. Schilirò, R. Lo Nigro, I. Deretzis, A. La Magna, F. Roccaforte, F. Iucolano, S. Ravesi, E. Frayssinet *et al.*, *ACS Appl. Electron. Mater.* **1**, 2342–2354 (2019). 364
- 329 ¹⁹S. E. Panasci, E. Schilirò, G. Greco, M. Cannas, F. M. Gelardi, S. Agnello, F. Roccaforte, and F. Giannazzo, *ACS Appl. Mater. Interfaces* **13**, 31248–31259 (2021). 365
- 330 ²⁰C. Lee, H. Yan, L. E. Brus, T. F. Heinz, J. Hone, and S. Ryu, *ACS Nano* **4**, 2695–2700 (2010). 366
- 331 ²¹J. Xu, L. Chen, Y.-W. Dai, Q. Cao, Q.-Q. Sun, S.-J. Ding, H. Zhu, and D. W. Zhang, *Sci. Adv.* **3**, e1602246 (2017). 367
- 332 ²²B. Chakraborty, A. Bera, D. V. S. Muthu, S. Bhowmick, U. V. Waghmare, and A. K. Sood, *Phys. Rev. B* **85**, 161403 (2012). 368
- 333 ²³D. Lloyd, X. Liu, J. W. Christopher, L. Cantley, A. Wadehra, B. L. Kim, B. B. Goldberg, A. K. Swan, and J. S. Bunch, *Nano Lett.* **16**, 5836–5841 (2016). 369
- 334 ²⁴F. Giannazzo, G. Fisichella, A. Piazza, S. Agnello, and F. Roccaforte, *Phys. Rev. B* **92**, 081307(R) (2015). 370
- 335 ²⁵C. Gong, C. Huang, J. Miller, L. Cheng, Y. Hao, D. Cobden, J. Kim, R. S. Ruoff, R. M. Wallace, K. Cho, X. Xu, and Y. J. Chabal, *ACS Nano* **7**, 11350–11357 (2013). 371
- 336 ²⁶A. Bruix, J. A. Miwa, N. Hauptmann, D. Wegner, S. Ulstrup, S. S. Grønberg, C. E. Sanders, M. Dendzik, A. Grubisic Cabo, M. Bianchi, J. V. Lauritsen, A. A. Khajetoorians, B. Hammer, and P. Hofmann, *Phys. Rev. B* **93**, 165422 (2016). 372
- 337 ²⁷A. Molina-Sánchez, D. Sangalli, K. Hummer, A. Marini, and L. Wirtz, *Phys. Rev. B* **88**, 045412 (2013). 373
- 338 ²⁸K. F. Mak, C. Lee, J. Hone, J. Shan, and T. F. Heinz, *Phys. Rev. Lett.* **105**, 136805 (2010). 374
- 339 ²⁹A. Splendiani, L. Sun, Y. Zhang, T. Li, J. Kim, C.-Y. Chim, G. Galli, and F. Wang, *Nano Lett.* **10**, 1271–1275 (2010). 375
- 340 ³⁰K. F. Mak, K. He, C. Lee, G. H. Lee, J. Hone, T. F. Heinz, and J. Shan, *Nat. Mater.* **12**, 207–211 (2013). 376
- 341 ³¹K. Kheng, R. T. Cox, M. Y. d'Aubigné, F. Bassani, K. Saminadayar, and S. Tatarenko, *Phys. Rev. Lett.* **71**, 1752 (1993). 377
- 342 ³²N. Scheuschner, O. Ochedowski, A. M. Kaulitz, R. Gillen, M. Schleberger, and J. Maultzsch, *Phys. Rev. B* **89**, 125406 (2014). 378
- 343 ³³M. Drüppel, T. Deilmann, P. Krüger, and M. Rohlfing, *Nat. Commun.* **8**, 2117 (2017). 379
- 344 ³⁴Y. V. Zhumagulov, A. Vagov, D. R. Gulevich, P. E. Faria Junior, and V. Perebeinos, *J. Chem. Phys.* **153**, 044132 (2020). 380
- 345 381
- 346 382
- 347 383
- 348 384